Fault-Tolerant Multi-Qubit Geometric Entangling Gates Using Photonic Cat Qubits

Ye-Hong Chen,[1] Roberto Stassi,[1, 2] Wei Qin,[1] Adam Miranowicz,[1, 3] and Franco Nori[1, 4, 5]

[1] *Theoretical Quantum Physics Laboratory, RIKEN Cluster for Pioneering Research, Wako-shi, Saitama 351-0198, Japan*
[2] *Dipartimento di Scienze Matematiche e Informatiche,*
Scienze Fisiche e Scienze della Terra, Università di Messina, 98166, Messina, Italy
[3] *Institute of Spintronics and Quantum Information, Faculty of Physics,*
Adam Mickiewicz University, 61-614 Poznań, Poland
[4] *Department of Physics, University of Michigan, Ann Arbor, Michigan 48109-1040, USA*
[5] *RIKEN Center for Quantum Computing (RQC), Wako-shi, Saitama 351-0198, Japan*
(Dated: September 13, 2021)

We propose a protocol to implement multi-qubit geometric gates (i.e., the Mølmer-Sørensen gate) using photonic cat qubits. These cat qubits stored in high-Q resonators are promising for hardware-efficient universal quantum computing. Specifically, in the limit of strong two-photon drivings, phase-flip errors of the cat qubits are effectively suppressed, leaving only a bit-flip error to be corrected. A geometric evolution guarantees the robustness of the protocol against stochastic noise along the evolution path. Moreover, by changing detunings of the cavity-cavity couplings at a proper time, the protocol can be robust against control imperfections (e.g., the total evolution time) without introducing extra noises into the system. As a result, the gate can produce multi-mode entangled cat states in a short time with high fidelities.

Keywords: Cat qubit; Geometric gate; Parametric driving

Introduction.—Quantum computers promise to drastically outperform classical computers on certain problems, such as factoring and unstructured database searching [1–5]. Recent experiments with superconducting qubits [6] and photons [7] have already demonstrated quantum advantage. To perform useful large-scale quantum computation, fragile quantum states must be protected from errors, which arise due to their inevitable interaction with the environment [1–3]. Aiming at this problem, strategies for quantum error correction are continuously being developed in the past decades [5, 8–25]. For instance, because most noisy environments are only locally correlated, quantum information can be protected by employing non-locality using, e.g., entangled qubit states [8], spatial distance [10], and their combinations [21, 25]. Note that this strategy has been extended to states that are non-local in the phase space of an oscillator [5, 11–13, 17–20, 22, 26–34], such as Schrödinger's cat states [12, 13, 35–40]. Encoding quantum information in such bosonic states has the benefit of involving fewer physical components. In particular, a cat qubit experiences only bit-flip noise, while the phase flip is exponentially suppressed. Additional layers of error correction can focus only on the bit-flip error, so that the number of building blocks can be significantly reduced [11, 24, 41].

In this manuscript, we propose to use cat qubits to implement multi-qubit geometric gates, i.e., the well-known Mølmer-Sørensen (MS) entangling gate [42, 43] and its multi-qubit generalizations [44]. Generally, the MS gate is a two-qubit geometric gate possessing a built-in noise-resilience feature against certain types of local noises [45–51]. It is also a significant resource for Grover's quantum search algorithm [3, 52] without

a third ancilla bit [53]. Previous works [54–63] implementing the MS gate using physical qubits (such as trapped ions and atoms) may experience various errors including bit flips, phase flips, qubit dephasing, etc. Thus, a huge physical resource is needed to correct the various errors [56, 64–66]. This requirement has driven researchers to optimize such implementations with respect to speed and robustness to nonideal control environments using extra control fields [60–63]. However, additional control fields may induce extra noises which should be corrected by using additional physical resources. All the above factors impede in scaling up the number of qubits because error channels increase when the number of physical qubits increases.

Instead, cat qubits, which experience only a bit-flip error, can be an excellent choice to overcome the above problems. We use a simple operation by once changing the detuning of cavity-cavity couplings during the evolution to suppress the influence of parameter imperfections (e.g., control imperfections in the gate time) without introducing extra noises. Moreover, we suggest, using cavity and circuit quantum electrodynamics [24, 40, 67], to realize our protocol. This can avoid some problems in trapped-ion implementation, such as the limitation of the Lamb-Dicke parameter.

Model and effective Hamiltonian.—We consider that N Kerr-nonlinear resonators (a_1, a_2, ..., a_N) with a same frequency ω_c are simultaneously coupled to another resonator (a_0) with a frequency ω_0 [See Fig. 1(a)]. The interaction Hamiltonian is $H_{\mathrm{int}} = \sum_{n=1}^{N} J a_n a_0^{\dagger} \exp{(i\Delta t)} + \text{h.c.}$, where J is the intercavity coupling strength and $\Delta = \omega_0 - \omega_c$ is the detuning. Hereafter, we assume $\hbar = 1$. Each Kerr-nonlinear resonator is resonantly driven by a two-photon drive of
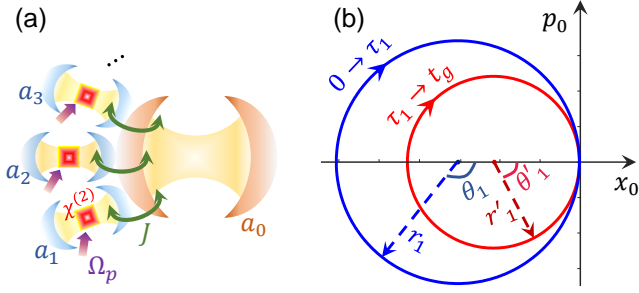
FIG. 1. (a) Schematic of N Kerr-nonlinear resonators coupled to another resonator. Driving the $\chi^{(2)}$ nonlinearity induce a two-photon driving in the cavity mode a_n. (b) Phase-space trajectories of the MS gate for $m = m' = 1$. The blue (red) circle denotes the trajectory of $\chi(t)$ when $t \in (0, \tau_1)$ [$t \in (\tau_1, t_g)$]. Here, $x_0 = (a_0 + a_0^\dagger)/\sqrt{2}$ and $p_0 = i(a_0^\dagger - a_0)/\sqrt{2}$ are the dimensionless position and momentum operators, respectively. We assume that the cavity mode a_0 is initially in its vacuum state.

FIG. 2. (a) Average infidelities $(1 - \bar{F}_N)$ of the N-qubit gates vs the period number $m = m'$ for $N = 2, 3, 4$. (b) Average gate fidelities $\bar{F}_2$ in the presence of stochastic noise. The blue dots (red crosses) denote the average fidelities when considering the stochastic errors of the coupling strength (detuning) for the noise parameter $\epsilon_s = 0.1$. We assume that $m = m' = 1$ and the noise affects the evolution 1,000 times. Other parameters are $J = 0.05K$, $\Delta = 2\sqrt{6m}J\alpha$, and $\Delta' = 4\sqrt{3m'}J\alpha$, resulting in $\beta(t_g) = -\pi/2$.

frequency ω_p and amplitude Ω_p, i.e., $\omega_c = \omega_p/2$ [24, 67]. The total Hamiltonian of the system in the interaction picture reads $H = \sum_{n=1}^{N} H_n^{\text{Kerr}} + H_{\text{int}}$. Here,

$$H_n^{\text{Kerr}} = -K a_n^{\dagger 2} a_n^2 + \left(\Omega_p a_n^2 + \text{h.c.}\right), \tag{1}$$

describes the two-photon driven Kerr nonlinearity, and K is the Kerr nonlinearity [68, 69]. Clearly, the coherent states $| \pm \alpha \rangle_n$ ($\alpha = \sqrt{\Omega_p/K}$) of the cavity mode a_n or, equivalently, the even and odd Schrödinger's cat states $|\mathcal{C}_\pm\rangle_n = \mathcal{N}_\pm (|\alpha\rangle_n \pm |-\alpha\rangle_n)$ are degenerate eigenstates of the Hamiltonian H_n^{Kerr} [67]. Here, $\mathcal{N}_\pm$ are normalization coefficients. For simplicity, we choose $\{K, \Omega_p, J, \Delta\} > 0$. Henceforth, these Kerr resonators are referred as pumped-cat oscillators (PCOs) [24, 67].

The orthogonal cat states $|\mathcal{C}_\pm\rangle_n$ can span a cat subspace $\mathcal{C}$, which is separated from the rest of the Hilbert space $\mathcal{C}_\perp$ by an energy gap $E_{\text{gap}} \simeq 4K\alpha^2$. When $J \ll E_{\text{gap}}$, the evolution of the cavity mode a_n is restricted in $\mathcal{C}$. Thus, we can define the raising and lowering operators as $\sigma_n^+ = |\mathcal{C}_-\rangle\langle\mathcal{C}_+|$ and $\sigma_n^- = (\sigma_n^+)^\dagger$, respectively. For $\alpha > \sqrt{2}$, we obtain $a_n|\mathcal{C}_\pm\rangle_n \simeq \alpha|\mathcal{C}_\mp\rangle_n$, and then the effective MS interaction:

$$H_{\text{eff}} \simeq 2J\alpha S_x \left[\exp\left(-i\Delta t\right)a_0 + \text{h.c.}\right], \tag{2}$$

where $S_x = \frac{1}{2}\sum_n (\sigma_n^+ + \sigma_n^-)$. We have dropped the terms regarding $\mathbb{1}_n = \sigma_n^+ \sigma_n^- + \sigma_n^- \sigma_n^+$.

Implementing MS gates.—The integral of H_{eff} can be calculated exactly [43],

$$U_{\text{MS}}(t) = \exp\left[-i\chi(t)a_0^\dagger S_x + \text{h.c.}\right] \exp\left[-i\beta(t)S_x^2\right],$$

where $\chi(t) = 2iJ\alpha[1 - \exp(i\Delta t)]/\Delta$ and $\beta(t) = (\sin\Delta t - \Delta t)(2J\alpha/\Delta)^2$. One observes that in the phase space $\chi(t)$ draws circles with a radius $r_m = 2J\alpha/\Delta$ and a rotation angle $\theta_m = \Delta\tau_m$ when $t = \tau_m = 2m\pi/\Delta$
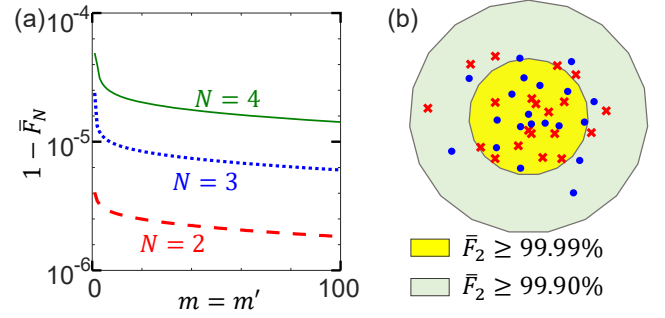
($m = 0, 1, 2, \ldots$). Thus, the cavity mode a_0 evolves along a circle in phase space and returns to its (arbitrary) initial state after m periods [see the blue-solid circle in Fig. 1(b)]. Meanwhile, $\beta(\tau_m)$ can be expressed by the area A enclosed by $\chi(t)$ as $\beta(\tau_m) = -2m\pi r_m^2 = -2mA$, i.e., a geometric phase. Note that an imperfection in the control time can cause a deviation in the area A, which is proportional to r_m^2. For the robustness against potential control imperfections, we can reduce the radius by changing the detuning $\Delta \to \Delta'$ at the time τ_m. The radius becomes $r_{m'}' = 2J\alpha/\Delta'$ ($m' = 0, 1, 2, \ldots$) and the rotation angle becomes $\theta_{m'}' = \Delta'\tau_{m'}'$ [see the red-solid circle in Fig. 1(b)]. The period numbers m and m' cannot both be zero. Hence, at the gate time $t_g = \tau_m + \tau_{m'}'$ with $\tau_{m'}' = 2m'\pi/\Delta'$, we have $\chi(t_g) = 0$, $\beta(t_g) = -2\pi\left(mr_m^2 + m'r_{m'}'^2\right)$, and the evolution operator

$$U_{\text{MS}}(t_g) = \exp\left[-i\beta(t_g)S_x^2\right]. \tag{3}$$

In particular, when $\beta(t_g) = -\pi/2$ and N is even, $U_{\text{MS}}(\tau_m)$ accomplishes the transformations:

$$\bigotimes_{n=1}^{N} |\mathcal{C}_\pm\rangle_n \xrightarrow{U_{\text{MS}}(t_g)} \frac{1}{\sqrt{2}} \left(\bigotimes_{n=1}^{N} |\mathcal{C}_\pm\rangle_n + i\bigotimes_{n=1}^{N} |\mathcal{C}_\mp\rangle_n\right),$$

which transforms product states (i.e., the input state $|\psi_{\text{in}}\rangle$) into maximally entangled cat states (i.e., the output state $|\psi_{\text{out}}\rangle$). Accompanied by single-qubit rotations [70–74], the MS gate can be applied in Grover's quantum search algorithm for both the marking and state amplification steps [53, 75]. The generation of input states in a PCO has been experimentally realized [70, 76]. For instance, using time-dependent two-photon drivings, one can generate a cat state with a fidelity $\gtrsim 95\%$ [67, 74, 77, 78] in the presence of decoherence.
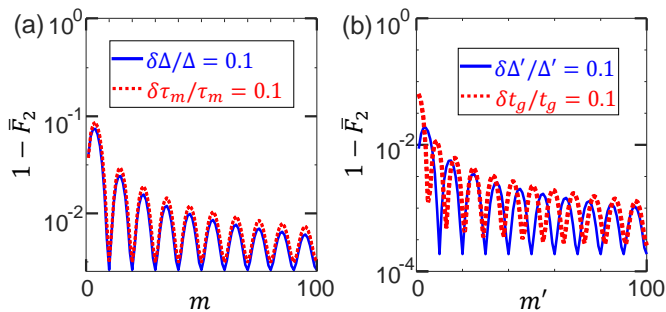
FIG. 3. Average infidelities of the two-qubit gate vs the period number: (a) m for $m' = 1$, and (b) m' for $m = 1$. Other parameters are the same as those in Fig. 2.
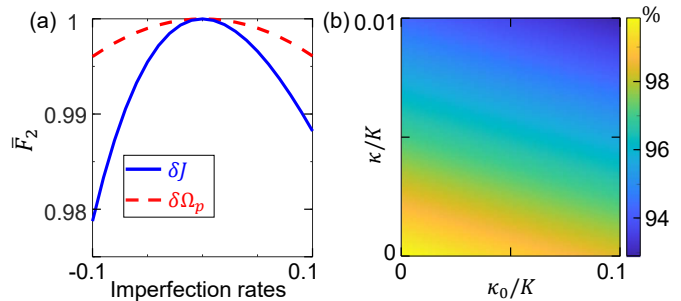

FIG. 4. (a) Average fidelities of the two-qubit gate vs imperfection rates $\delta J/J$ and $\delta\Omega_p/\Omega_p$ when $J = 0.05K$ and arbitrary period number m, m'. (b) Fidelity $F_{\text{out}} = \langle\psi_{\text{out}}|\rho(t_g)|\psi_{\text{out}}\rangle$ of the output state $|\psi_{\text{out}}\rangle$ vs single-photon decay rates κ_0 and κ, when $m = 1$, $m' = 10$ and $J = K$. Other parameters are $\alpha = 2$, $\epsilon_a = -\delta t_g/t_g = 0.1$, and $\beta(t_g) = -\pi/2$. The detunings satisfy the condition $\epsilon_a m\Delta' = (1 - \epsilon_a)m'\Delta$.

The average fidelity of an N-qubit gate over all possible initial states is defined by $\bar{F}_N = \left[\text{Tr}(MM^\dagger) + |\text{Tr}(M)|^2\right]/(D^2 + D)$ [79, 80] with $M = \mathcal{P}_c U_{\text{MS}}^\dagger \exp\left(-iHt_g\right)\mathcal{P}_c$. Here, $\mathcal{P}_c$ (D) is the projector (dimension) of the computing subspace. For a large m (m') (corresponding to a large detuning), we notice from Fig. 2(a) that $\bar{F}_N > 99.99\%$. This is because a large detuning can minimize the possibility of photon leakage to the subspace $\mathcal{C}_\perp$. Note that such a leakage possibility may slightly accumulate when the qubit number increases. Thus, to implement multi-qubit MS gates with high fidelities, one needs a smaller coupling strength or a larger detuning. For simplicity, the following discussions focus on $N = 2$.

Stochastic noise.—A geometric gate is path-independent, thus is robust against stochastic errors along the evolution path. In the presence of stochastic errors, a parameter $*$ should be corrected as $* = *[1 \pm \text{rand}(\epsilon_s)]$, where the function $\text{rand}(\epsilon_s)$ generates a random number in the interval $(0, \epsilon_s)$. As shown in Fig. 2(b), stochastic noise does not significantly affect the gate fidelity. We can see $F_2 > 99.9\%$ when considering stochastic errors in coupling strength and detuning.

Parameter imperfections.—Now we consider the effects of the imperfection of a parameter $*$, as $\delta* = (*_a - *)$, where $*_a$ ($*$) denotes the actual (ideal) value. Obviously, the deviations of the radius r_m ($r'_{m'}$) affect the geometric phase $\beta(t_g)$, but not the excitation number of the cavity mode a_0 at the time t_g. In contrast, the deviations of the rotation angle θ_m ($\theta'_{m'}$) affect both. When m' is fixed, increasing m can suppress the influence of imperfections in the parameters $\{\Delta, \tau_m\}$ [see Fig. 3(a)]. Similarly, by increasing m', our protocol is robust against parameter imperfections $\delta\Delta'$ and δt_g [see Fig. 3(b)]. This is because a large period number m (m'), corresponding to a large detuning Δ (Δ'), can shorten the radius r_m ($r'_{m'}$) for $\Delta = 2\sqrt{6m}J\alpha$ ($\Delta' = 4\sqrt{3m'}J\alpha$). Thus, the distance between the evolution state and the original coordinates (i.e., the target state) in phase space becomes very short

[e.g., see the circles in Fig. 1(b)].

Furthermore, for imperfections in the gate time t_g, we can choose $\tau'_{m'}/t_g = \text{Max}\left(|\delta t_g/t_g|\right) = \epsilon_a$ leading to

$$t_g = \sqrt{\pi|\beta(t_g)|} \cdot \left[\sqrt{2}J\alpha\sqrt{(1-\epsilon_a)^2/m + \epsilon_a^2/m'}\right]^{-1},$$

which is mostly independent of m' for $m' \gg m$. One can arbitrarily choose m' for robustness against imperfections in the gate time without increasing the total evolution time. Hence, we use these parameters hereafter. Because the parameters $\{J, \Omega_p\}$ affect only the radius r_m ($r'_{m'}$), imperfections in these parameters weakly affect affect the gate fidelity. In the presence of such imperfections, $\chi(t_g) = 0$ holds, and $\beta(t_g) \to \beta_a(t_g) \simeq \beta(t_g)(1 + \delta J)(1 + \delta\Omega_p/2)$, which is independent of m and m'. For imperfection rates $\delta J/J = \delta\Omega_p/\Omega_p = \pm 0.1$, the gate fidelity remains $\bar{F}_2 \geq 98\%$ [see Fig. 4(a)].

Single-photon loss.—A major source of noise in a resonator is single-photon loss. When it is considered, the system dynamics is described by the Lindblad master equation $\dot\rho = -i[H,\rho] + \sum_{j=0}^N \kappa_j \mathcal{D}[a_j]\rho$, where $\mathcal{D}[o]\rho = o\rho o^\dagger - \left(o^\dagger o\rho + \rho o^\dagger o\right)/2$ is the standard Lindblad superoperator and κ_j is the single-photon loss rate of the jth cavity mode. For simplicity, we choose $\kappa_n = \kappa$ and an initial state $|\psi_{\text{in}}\rangle = |0\rangle_0 \bigotimes_{n=1}^N |\mathcal{C}_+\rangle_n$. The fidelity $F_{\text{out}} = \langle\psi_{\text{out}}|\rho(t_g)|\psi_{\text{out}}\rangle$ of the output state vs the single-photon decays is shown in Fig. 4(b). Because the cavity mode a_0 can be adiabatically eliminated for a large detuning, the system is mostly insensitive to the single-photon loss of the cavity mode a_0.

The single-photon loss in the PCOs has a greater influence on the gate fidelity than that of the cavity mode a_0 [see Fig. 4(b)]. When system-bath coupling is smaller than the energy gap E_{gap}, the dynamics of the cat qubits is still approximatively confined to the subspace $\mathcal{C}$. This is confirmed in Fig. 5(a), which shows the no-leakage probability $P_\mathcal{C} = \sum_n {}_n\langle\mathcal{C}_+|\rho(t_g)|\mathcal{C}_+\rangle_n + {}_n\langle\mathcal{C}_-|\rho(t_g)|\mathcal{C}_-\rangle_n$.

In this restricted subspace, the effective master equation becomes

$$\dot{\rho}_{\text{eff}} \simeq -i[H, \rho_{\text{eff}}] + \kappa_0 \mathcal{D}[a_0]\rho_{\text{eff}}$$
$$+ \frac{\kappa \alpha^2}{\sqrt{1 - e^{-4\alpha^2}}} \sum_{n=1}^{N} \mathcal{D}[\sigma_n^x + i e^{-2\alpha^2}\sigma_n^y]\rho_{\text{eff}}, \quad (4)$$

where $\sigma_n^x = \sigma_n^+ + \sigma_n^-$ and $\sigma_n^y = i(\sigma_n^- - \sigma_n^+)$. This means that in the computing subspace the single-photon loss can lead primarily to a bit-flip error (σ_n^x), which is accompanied by an exponentially small phase-flip error (σ_n^y) [24].

For $\alpha > \sqrt{2}$, the phase-flip error can be neglected, leaving only the bit-flip error. As shown in Fig. 5(a), the full dynamics (blue-dotted curve) is in excellent agreement with the effective one (red-solid curve). This is because a large distance of the coherent states $|\pm\alpha\rangle_n$ in the phase space can ensure protection against any noise process that causes local displacements in the phase space. For $\alpha^2 \gtrsim 3$, the bit-flip error rate $\kappa\alpha^2$ increases linearly with the photon number, which becomes a kind of "biased noise" [81]. Such noise is an important resource in fault-tolerant quantum computation [81, 82], because it can reduce the number of building blocks for error-correction codes by focusing strongly on the remaining bit-flip error [24].

Pure dephasing.—In the presence of white dephasing noise, we need to add the term $\sum_{j=0}^{N} \gamma_j \mathcal{D}[a_j^\dagger a_j]\rho$ to the master equation, where γ_j is the dephasing rate of the jth cavity mode. Same as above, we assume $\gamma_n = \gamma$. In the cat subspace, pure dephasing does not affect the system dynamics because the operator $a_n^\dagger a_n$ in this subspace can be expressed as $a_n^\dagger a_n \Rightarrow \alpha^2 \mathbb{1}_n$ when $\alpha > \sqrt{2}$. However, because $_n\langle\psi_\pm^e|a_n^\dagger a_n|\mathcal{C}_\pm\rangle_n \sim \alpha$ [83], the operator $a_n^\dagger a_n$ causes photon leakage to the subspace $\mathcal{C}_\perp$ with a rate $\gamma\alpha^2$ [24].

We notice from Fig. 5(b) that $P_\mathcal{C} \simeq F_{\text{out}}$ when $\gamma_0 = 0$ and $\gamma = 0.01K$, indicating that the leakage is mainly caused by the pure dephasing in the PCOs. When $\gamma_0 = 0.1K$, F_{out} slightly decreases [see the red-dashed curve in Fig. 5(b)], while $P_\mathcal{C}$ remains mostly unchanged [see the blue squares and red crosses in Fig. 5(b)]. The pure dephasing γ_0 does not cause photon leakage but slightly decreases ($\sim 1\%$ when $\gamma_0 = 0.1K$) the output-state fidelity.

Discussion.—Superconducting circuits [70, 76, 84, 85] can be a possible implementation of the PCOs. For instance, one can use the Josephson parametric amplifier [4, 5, 74, 86–96] to realize the Hamiltonian H_n^{Kerr}. Another especially promising setup to realize our protocol could be a single junction or transmon embedded in a 3D oscillator [97]. The Kerr nonlinearity and the two-photon drive can be respectively realized by the Josephson junction (transmon) nonlinearity and four-wave mixing [24, 98–101]. In such experimental setups, current experiments [70, 76, 102, 103] have
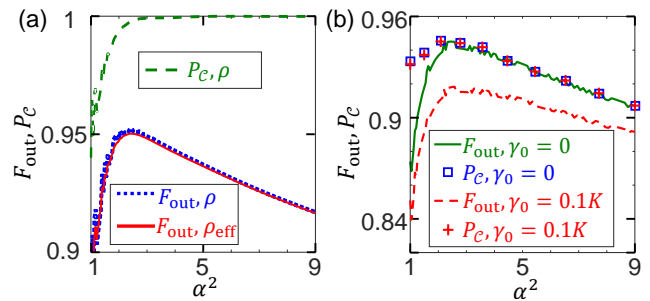

FIG. 5. Fidelity F_{out} and no-leakage probability $P_\mathcal{C}$ vs α^2 when considering: (a) single-photon loss and (b) pure dephasing. For (a), the red-solid curve is calculated from the effective master equation in Eq. (4) when neglecting the σ_y terms. We assume $\kappa_0 = 0$ and $\kappa = 0.01K$. The imperfection rate of the gate time is $\epsilon_a = -\delta t_g/t_g = 0.1$. For (b), we assume $\epsilon_a = \kappa_0 = \kappa = 0$ to focus on the influence of pure dephasing with a rate $\gamma = 0.01K$. Other parameters are the same as those in Fig. 4(b).

achieved the intensity of a two-photon drive $\Omega_p/2\pi \sim$ 20–50 MHz and a Kerr nonlinearity $K/2\pi \sim$ 1–10 MHz. Hence, by choosing $m = 1$, $m' = 10$, $J = K$, and $\epsilon_a = -\delta t_g/t_g = 0.1$, the gate time of our protocol for $N = 2$ qubits is $t_g \sim 14$ ns. The gate time may slightly increase when the qubit number increases, but it is still much shorter compared to the lifetime $\gtrsim 5$ μs of a superconducting cavity mode [19, 20, 33, 70, 104–107]. Using these realistic parameters, the fidelity of the output state (i.e., large-amplitude multi-mode entangled cat states) for two qubits can reach $\gtrsim 96\%$.

Conclusions.—We have investigated the possibility of using photonic cat qubits for the implementation of multi-qubit geometric gates, which can rapidly generate maximally multi-mode entangled cat states with high fidelities. Our protocol is robust against stochastic noise along the evolution path because of the character of the geometric evolution. By increasing the detuning at a suitable time, the protocol can tolerate imperfections in the detuning and the gate time. For a large amplitude α, the phase-flip error can be exponentially suppressed, leaving only the bit-flip error. The pure dephasing of the cavity modes may lead to the photon leakage out of the computing subspace, but does not cause qubit-dephasing problems for the system. Therefore, error-correction layers can focus on only the bit-flip error using less physical resources. In summary, our results offer a realistic and hardware-efficient method for multi-qubit fault-tolerant quantum computation.

———————————

[1] J. D. Hidary, *Quantum Computing: An Applied Approach* (Springer, Berlin, 2019).

[2] R. J. Lipton and K. W. Regan, *Introduction to Quantum Algorithms via Linear Algebra* (The MIT Press, Cambridge, 2021).

[3] M. A. Nielsen and I. L. Chuang, *Quantum Computation and Quantum Information* (Cambridge Univ. Press, Cambridge, 2000).

[4] A. F. Kockum and F. Nori, "Quantum bits with Josephson junctions," in *Fundamentals and Frontiers of the Josephson Effect*, Vol. 286, edited by F. Tafuri (Springer, Berlin, 2019) Chap. 17, pp. 703–741.

[5] M. Kjaergaard, M. E. Schwartz, J. Braumüller, P. Krantz, J. I.-J. Wang, S. Gustavsson, and W. D. Oliver, "Superconducting qubits: Current state of play," Ann. Rev. Cond. Matt. Phys. **11**, 369–395 (2020).

[6] F. Arute *et al.*, "Quantum supremacy using a programmable superconducting processor," Nature (London) **574**, 505–510 (2019).

[7] H.-S. Zhong *et al.*, "Quantum computational advantage using photons," Science **370**, 1460–1463 (2020).

[8] P. W. Shor, "Scheme for reducing decoherence in quantum computer memory," Phys. Rev. A **52**, R2493–R2496 (1995).

[9] A. Steane, "Multiple-particle interference and quantum error correction," Proc. Roy. Soc. Lond. A **452**, 2551–2577 (1996).

[10] A. Y. Kitaev, "Fault-tolerant quantum computation by anyons," Ann. Phys. **303**, 2–30 (2003).

[11] D. Gottesman, A. Kitaev, and J. Preskill, "Encoding a qubit in an oscillator," Phys. Rev. A **64**, 012310 (2001).

[12] T. C. Ralph, A. Gilchrist, G. J. Milburn, W. J. Munro, and S. Glancy, "Quantum computation with optical coherent states," Phys. Rev. A **68**, 042319 (2003).

[13] A. Gilchrist, K. Nemoto, W. J. Munro, T. C. Ralph, S. Glancy, S. L. Braunstein, and G. J. Milburn, "Schrödinger cats and their power for quantum information processing," J. Opt. B **6**, S828–S833 (2004).

[14] F. Gaitan, *Quantum Error Correction and Fault Tolerant Quantum Computing* (CRC Press, Boca Raton, 2008).

[15] D. A. Lidar and T. A. Brun, eds., *Quantum Error Correction* (Cambridge Univ. Press, New York, 2013).

[16] D. Gottesman, "An introduction to quantum error correction and fault-tolerant quantum computation," in *Quantum Information Science and Its Contributions to Mathematics, Proceedings of Symposia in Applied Mathematics*, Vol. 68 (American Mathematical Society, Washington, DC, 2010) Chap. 3, pp. 13–58.

[17] C. Chamberland *et al.*, "Building a fault-tolerant quantum computer using concatenated cat codes," arXiv:2012.04108 (2020).

[18] M. Mirrahimi, "Cat-qubits for quantum computation," Comptes Rendus Phys. **17**, 778–787 (2016).

[19] W. Cai, Y. Ma, W. Wang, C.-L. Zou, and L. Sun, "Bosonic quantum error correction codes in superconducting quantum circuits," Fund. Res. **1**, 50–67 (2021).

[20] W.-L. Ma, S. Puri, R. J. Schoelkopf, M. H. Devoret, S. M. Girvin, and L. Jiang, "Quantum control of bosonic modes with superconducting circuits," Sci. Bull. **66**, 1789–1805 (2021).

[21] A. G. Fowler, M. Mariantoni, J. M. Martinis, and A. N. Cleland, "Surface codes: Towards practical large-scale quantum computation," Phys. Rev. A **86**, 032324 (2012).

[22] M. Mirrahimi, Z. Leghtas, V. V. Albert, S. Touzard, R. J. Schoelkopf, L. Jiang, and M. H. Devoret, "Dynamically protected cat-qubits: a new paradigm for universal quantum computation," New J. Phys. **16**, 045014 (2014).

[23] J. Zhang, S. J. Devitt, J. Q. You, and F. Nori, "Holonomic surface codes for fault-tolerant quantum computation," Phys. Rev. A **97**, 022335 (2018).

[24] S. Puri, A. Grimm, P. Campagne-Ibarcq, A. Eickbusch, K. Noh, G. Roberts, L. Jiang, M. Mirrahimi, M. H. Devoret, and S. M. Girvin, "Stabilized cat in a driven nonlinear cavity: A fault-tolerant error syndrome detector," Phys. Rev. X **9**, 041009 (2019).

[25] D. Litinski, "A game of surface codes: Large-scale quantum computing with lattice surgery," Quantum **3**, 128 (2019).

[26] V. V. Albert, C. Shu, S. Krastanov, C. Shen, R.-B. Liu, Z.-B. Yang, R. J. Schoelkopf, M. Mirrahimi, M. H. Devoret, and L. Jiang, "Holonomic quantum control with continuous variable systems," Phys. Rev. Lett. **116**, 140502 (2016).

[27] M. H. Michael, M. Silveri, R. T. Brierley, V. V. Albert, J. Salmilehto, L. Jiang, and S. M. Girvin, "New class of quantum error-correcting codes for a bosonic mode," Phys. Rev. X **6**, 031006 (2016).

[28] R. W. Heeres, P. Reinhold, N. Ofek, L. Frunzio, L. Jiang, M. H. Devoret, and R. J. Schoelkopf, "Implementing a universal gate set on a logical qubit encoded in an oscillator," Nat. Commun. **8**, 94 (2017).

[29] L. Li, C.-L. Zou, V. V. Albert, S. Muralidharan, S. M. Girvin, and L. Jiang, "Cat codes with optimal decoherence suppression for a lossy bosonic channel," Phys. Rev. Lett. **119**, 030502 (2017).

[30] K. S. Chou, J. Z. Blumoff, C. S. Wang, P. C. Reinhold, C. J. Axline, Y. Y. Gao, L. Frunzio, M. H. Devoret, L. Jiang, and R. J. Schoelkopf, "Deterministic teleportation of a quantum gate between two logical qubits," Nature (London) **561**, 368–373 (2018).

[31] S. Rosenblum, Y. Y. Gao, P. Reinhold, C. Wang, C. J. Axline, L. Frunzio, S. M. Girvin, L. Jiang, M. Mirrahimi, M. H. Devoret, and R. J. Schoelkopf, "A CNOT gate between multiphoton qubits encoded in two cavities," Nat. Commun. **9**, 652 (2018).

[32] V. V. Albert, S. O. Mundhada, A. Grimm, S. Touzard., M. H. Devoret, and L. Jiang, "Pair-cat codes: autonomous error-correction with low-order nonlinearity," Quantum Sci. Tech. 4, 035007 (2019).

[33] Y. Xu, Y. Ma, W. Cai, X. Mu, W. Dai, W. Wang, L. Hu, X. Li, J. Han, H. Wang, Y. P. Song, Z.-B. Yang, S.-B. Zheng, and L. Sun, "Demonstration of controlled-phase gates between two error-correctable photonic qubits," Phys. Rev. Lett. 124, 120501 (2020).

[34] J. M. Gertler, B. Baker, J. Li, S. Shirol, J. Koch, and C. Wang, "Protecting a bosonic qubit with autonomous quantum error correction," Nature (London) 590, 243–248 (2021).

[35] V. V. Dodonov, I. A. Malkin, and V. I. Man'ko, "Even and odd coherent states and excitations of a singular oscillator," Physica 72, 597–615 (1974).

[36] Y.-x. Liu, L. F. Wei, and F. Nori, "Preparation of macroscopic quantum superposition states of a cavity field via coupling to a superconducting charge qubit," Phys. Rev. A 71, 063820 (2005).

[37] M. Kira, S. W. Koch, R. P. Smith, A. E. Hunter, and S. T. Cundiff, "Quantum spectroscopy with Schrödinger-cat states," Nat. Phys. 7, 799–804 (2011).

[38] J. Gribbin, Computing with Quantum Cats: From Colossus to Qubits (Bantam Press, London, 2013).

[39] Y.-H. Chen, W. Qin, R. Stassi, X. Wang, and F. Nori, "Fast binomial-code holonomic quantum computation with ultrastrong light-matter coupling," arXiv:2012.06090 (Phys. Rev. Research, in process) (2021).

[40] Y.-H. Chen, W. Qin, X. Wang, A. Miranowicz, and F. Nori, "Shortcuts to adiabaticity for the quantum Rabi model: Efficient generation of giant entangled cat states via parametric amplification," Phys. Rev. Lett. 126, 023602 (2021).

[41] J. Guillaud and M. Mirrahimi, "Repetition cat qubits for fault-tolerant quantum computation," Phys. Rev. X 9, 041053 (2019).

[42] A. Sørensen and K. Mølmer, "Quantum computation with ions in thermal motion," Phys. Rev. Lett. 82, 1971–1974 (1999).

[43] A. Sørensen and K. Mølmer, "Entanglement and quantum computation with ions in thermal motion," Phys. Rev. A 62, 022311 (2000).

[44] K. Mølmer and A. Sørensen, "Multiparticle entanglement of hot trapped ions," Phys. Rev. Lett. 82, 1835–1838 (1999).

[45] P. Solinas, P. Zanardi, and N. Zanghì, "Robustness of non-Abelian holonomic quantum gates against parametric noise," Phys. Rev. A 70, 042316 (2004).

[46] S.-L. Zhu and P. Zanardi, "Geometric quantum gates that are robust against stochastic control errors," Phys. Rev. A 72, 020301(R) (2005).

[47] S.-B. Zheng, "Unconventional geometric quantum phase gates with a cavity QED system," Phys. Rev. A 70, 052320 (2004).

[48] S.-B. Zheng, C.-P. Yang, and F. Nori, "Comparison of the sensitivity to systematic errors between nonadiabatic non-Abelian geometric gates and their dynamical counterparts," Phys. Rev. A 93, 032313 (2016).

[49] C. Song, S.-B. Zheng, P. Zhang, K. Xu, L. Zhang, Q. Guo, W. Liu, D. Xu, H. Deng, K. Huang, D. Zheng, X. Zhu, and H. Wang, "Continuous-variable geometric phase and its manipulation for quantum computation in a superconducting circuit," Nat. Commun. 8, 1061 (2017).

[50] Z.-Y. Xue, F.-L. Gu, Z.-P. Hong, Z.-H. Yang, D.-W. Zhang, Y. Hu, and J. Q. You, "Nonadiabatic holonomic quantum computation with dressed-state qubits," Phys. Rev. Appl. 7, 054022 (2017).

[51] Y.-H. Kang, Y.-H. Chen, Z.-C. Shi, B.-H. Huang, J. Song, and Y. Xia, "Nonadiabatic holonomic quantum computation using Rydberg blockade," Phys. Rev. A 97, 042336 (2018).

[52] L. K. Grover, "Quantum mechanics helps in searching for a needle in a haystack," Phys. Rev. Lett. 79, 325–328 (1997).

[53] K.-A. Brickman, P. C. Haljan, P. J. Lee, M. Acton, L. Deslauriers, and C. Monroe, "Implementation of Grover's quantum search algorithm in a scalable system," Phys. Rev. A 72, 050306(R) (2005).

[54] P. C. Haljan, K.-A. Brickman, L. Deslauriers, P. J. Lee, and C. Monroe, "Spin-dependent forces on trapped ions for phase-stable quantum gates and entangled states of spin and motion," Phys. Rev. Lett. 94, 153602 (2005).

[55] G. Kirchmair, J. Benhelm, F. Zähringer, R. Gerritsma, C. F. Roos, and R. Blatt, "Deterministic entanglement of ions in thermal states of motion," New J. Phys. 11, 023002 (2009).

[56] D. Hayes, S. M. Clark, S. Debnath, D. Hucul, I. V. Inlek, K. W. Lee, Q. Quraishi, and C. Monroe, "Coherent error suppression in multiqubit entangling gates," Phys. Rev. Lett. 109, 020503 (2012).

[57] A. Lemmer, A. Bermudez, and M. B. Plenio, "Driven geometric phase gates with trapped ions," New J. Phys. 15, 083001 (2013).

[58] F. Haddadfarshi and F. Mintert, "High fidelity quantum gates of trapped ions in the presence of motional heating," New J. Phys. 18, 123007 (2016).

[59] H. Takahashi, P. Nevado, and M. Keller, "Mølmer-Sørensen entangling gate for cavity QED systems," J. Phys. B 50, 195501 (2017).

[60] Y. Shapira, R. Shaniv, T. Manovitz, N. Akerman, and R. Ozeri, "Robust entanglement gates for trapped-ion qubits," Phys. Rev. Lett. 121, 180502 (2018).

[61] T. Manovitz, A. Rotem, R. Shaniv, I. Cohen, Y. Shapira, N. Akerman, A. Retzker, and R. Ozeri, "Fast dynamical decoupling of the Mølmer-Sørensen entangling gate," Phys. Rev. Lett. 119, 220505 (2017).

[62] A. Mitra, M. J. Martin, G. W. Biedermann, A. M. Marino, P. M. Poggi, and I. H. Deutsch, "Robust Mølmer-Sørensen gate for neutral atoms using rapid adiabatic Rydberg dressing," Phys. Rev. A 101, 030301(R) (2020).

[63] Y. Wang, J.-L. Wu, J.-X. Han, Y.-Y. Jiang, Y. Xia, and J. Song, "Resilient Mølmer-Sørensen gate with cavity QED," Phys. Lett. A 388, 127033 (2021).

[64] H. Haffner, C. Roos, and R. Blatt, "Quantum computing with trapped ions," Phys. Rep. 469, 155–203 (2008).

[65] C. D. Bruzewicz, J. Chiaverini, R. McConnell, and J. M. Sage, "Trapped-ion quantum computing: Progress and challenges," Appl. Phys. Rev. 6, 021314 (2019).

[66] P. Parrado-Rodríguez, C. Ryan-Anderson, A. Bermudez, and M. Müller, "Crosstalk suppression for fault-tolerant quantum error correction with trapped ions," Quantum 5, 487 (2021).

[67] S. Puri, S. Boutin, and A. Blais, "Engineering the

quantum states of light in a Kerr-nonlinear resonator by two-photon driving," npj Quantum Inf. **3**, 18 (2017).

[68] A. Miranowicz, J. Bajer, N. Lambert, Y.-x. Liu, and F. Nori, "Tunable multiphonon blockade in coupled nanomechanical resonators," Phys. Rev. A **93**, 013808 (2016).

[69] J. Bourassa, F. Beaudoin, Jay M. Gambetta, and A. Blais, "Josephson-junction-embedded transmission-line resonators: From Kerr medium to in-line transmon," Phys. Rev. A **86**, 013814 (2012).

[70] A. Grimm, N. E. Frattini, S. Puri, S. O. Mundhada, S. Touzard, M. Mirrahimi, S. M. Girvin, S. Shankar, and M. H. Devoret, "Stabilization and operation of a Kerr-cat qubit," Nature (London) **584**, 205–209 (2020).

[71] N. A. Masluk, I. M. Pop, A. Kamal, Z. K. Minev, and M. H. Devoret, "Microwave characterization of Josephson junction arrays: Implementing a low loss superinductance," Phys. Rev. Lett. **109**, 137002 (2012).

[72] I. M. Pop, K. Geerlings, G. Catelani, R. J. Schoelkopf, L. I. Glazman, and M. H. Devoret, "Coherent suppression of electromagnetic dissipation due to superconducting quasiparticles," Nature (London) **508**, 369–372 (2014).

[73] J. Cohen, W. C. Smith, M. H. Devoret, and M. Mirrahimi, "Degeneracy-preserving quantum nondemolition measurement of parity-type observables for cat qubits," Phys. Rev. Lett. **119**, 060503 (2017).

[74] See Supplemental Material including Refs. [3, 52, 53, 70–73, 95, 96] for detailed derivations and discussions of our main results.

[75] L. DiCarlo, J. M. Chow, J. M. Gambetta, L. S. Bishop, B. R. Johnson, D. I. Schuster, J. Majer, A. Blais, L. Frunzio, S. M. Girvin, and R. J. Schoelkopf, "Demonstration of two-qubit algorithms with a superconducting quantum processor," Nature (London) **460**, 240–244 (2009).

[76] Z. Leghtas, S. Touzard, I. M. Pop, A. Kou, B. Vlastakis, A. Petrenko, K. M. Sliwa, A. Narla, S. Shankar, M. J. Hatridge, M. Reagor, L. Frunzio, R. J. Schoelkopf, M. Mirrahimi, and M. H. Devoret, "Confining the state of light to a quantum manifold by engineered two-photon loss," Science **347**, 853–857 (2015).

[77] J. R. Johansson, P. D. Nation, and F. Nori, "QuTiP: An open-source Python framework for the dynamics of open quantum systems," Comp. Phys. Comm. **183**, 1760 (2012).

[78] J. R. Johansson, P. D. Nation, and F. Nori, "QuTiP 2: A Python framework for the dynamics of open quantum systems," Comp. Phys. Comm. **184**, 1234–1240 (2013).

[79] P. Zanardi and D. A. Lidar, "Purity and state fidelity of quantum channels," Phys. Rev. A **70**, 012315 (2004).

[80] L. H. Pedersen, N. M. Møller, and K. Mølmer, "Fidelity of quantum operations," Phys. Lett. A **367**, 47–51 (2007).

[81] P. Aliferis and J. Preskill, "Fault-tolerant quantum computation against biased noise," Phys. Rev. A **78**, 052331 (2008).

[82] D. K. Tuckett, S. D. Bartlett, and S. T. Flammia, "Ultrahigh error threshold for surface codes with biased noise," Phys. Rev. Lett. **120**, 050505 (2018).

[83] Here, $|\psi_{\pm}^e\rangle_n \in \mathcal{C}_\perp$ are orthogonal eigenstates of H_n^{Kerr}. The energy gap between the cat subspace and $|\psi_{\pm}^e\rangle_n$ is $E_{\mathrm{gap}} \simeq 4K\alpha^2$.

[84] E. Flurin, N. Roch, J. D. Pillet, F. Mallet, and B. Huard, "Superconducting quantum node for entanglement and storage of microwave radiation," Phys. Rev. Lett. **114**, 090503 (2015).

[85] W. Wustmann and V. Shumeiko, "Parametric resonance in tunable superconducting cavities," Phys. Rev. B **87**, 184501 (2013).

[86] P. D. Nation, J. R. Johansson, M. P. Blencowe, and F. Nori, "Colloquium: Stimulating uncertainty: Amplifying the quantum vacuum with superconducting circuits," Rev. Mod. Phys. **84**, 1–24 (2012).

[87] M. Wallquist, V. S. Shumeiko, and G. Wendin, "Selective coupling of superconducting charge qubits mediated by a tunable stripline cavity," Phys. Rev. B **74**, 224506 (2006).

[88] J.-Q. Liao, Z. R. Gong, L. Zhou, Y.-x. Liu, C. P. Sun, and F. Nori, "Controlling the transport of single photons by tuning the frequency of either one or two cavities in an array of coupled cavities," Phys. Rev. A **81**, 042304 (2010).

[89] Z.-L. Xiang, S. Ashhab, J. Q. You, and F. Nori, "Hybrid quantum circuits: Superconducting circuits interacting with other quantum systems," Rev. Mod. Phys. **85**, 623–653 (2013).

[90] O. Yaakobi, L. Friedland, C. Macklin, and I. Siddiqi, "Parametric amplification in Josephson junction embedded transmission lines," Phys. Rev. B **87**, 144301 (2013).

[91] C. Macklin, K. O'Brien, D. Hover, M. E. Schwartz, V. Bolkhovsky, X. Zhang, W. D. Oliver, and I. Siddiqi, "A near-quantum-limited Josephson traveling-wave parametric amplifier," Science **350**, 307–310 (2015).

[92] A. Roy and M. Devoret, "Introduction to parametric amplification of quantum signals with Josephson circuits," Comptes Rendus Phys. **17**, 740–755 (2016).

[93] X. Gu, A. F. Kockum, A. Miranowicz, Y. x. Liu, and F. Nori, "Microwave photonics with superconducting quantum circuits," Phys. Rep. **718-719**, 1–102 (2017).

[94] X. Wang, A. Miranowicz, and F. Nori, "Ideal quantum nondemolition readout of a flux qubit without purcell limitations," Phys. Rev. Appl. **12**, 064037 (2019).

[95] Z. Wang, M. Pechal, E. A. Wollack, P. Arrangoiz-Arriola, M. Gao, N. R. Lee, and A. H. Safavi-Naeini, "Quantum dynamics of a few-photon parametric oscillator," Phys. Rev. X **9**, 021049 (2019).

[96] S. Masuda, T. Ishikawa, Y. Matsuzaki, and S. Kawabata, "Controls of a superconducting quantum parametron under a strong pump field," Sci. Rep. **11** (2021).

[97] A. Megrant, C. Neill, R. Barends, B. Chiaro, Y. Chen, L. Feigl, J. Kelly, E. Lucero, M. Mariantoni, P. J. J. O'Malley, D. Sank, A. Vainsencher, J. Wenner, T. C. White, Y. Yin, J. Zhao, C. J. Palmstrøm, J. M. Martinis, and A. N. Cleland, "Planar superconducting resonators with internal quality factors above one million," Appl. Phys. Lett. **100**, 113510 (2012).

[98] Y.-H. Chen, W. Qin, and F. Nori, "Fast and high-fidelity generation of steady-state entanglement using pulse modulation and parametric amplification," Phys. Rev. A **100**, 012339 (2019).

[99] W. Qin, V. Macrì, A. Miranowicz, S. Savasta, and F. Nori, "Emission of photon pairs by mechanical stimulation of the squeezed vacuum," Phys. Rev. A **100**, 062501 (2019).

[100] W. Qin, Y.-H. Chen, X. Wang, A. Miranowicz, and

F. Nori, "Strong spin squeezing induced by weak squeezing of light inside a cavity," Nanophotonics **9**, 4853–4868 (2020).

[101] W. Qin, A. Miranowicz, H. Jing, and F. Nori, "Generating long-lived macroscopically distinct superposition states in atomic ensembles," Phys. Rev. Lett. **127**, 093602 (2021).

[102] S. Touzard, A. Kou, N. E. Frattini, V. V. Sivak, S. Puri, A. Grimm, L. Frunzio, S. Shankar, and M. H. Devoret, "Gated conditional displacement readout of superconducting qubits," Phys. Rev. Lett. **122**, 080502 (2019).

[103] Y. Y. Gao, B. J. Lester, Y. Zhang, C. Wang, S. Rosenblum, L. Frunzio, L. Jiang, S. M. Girvin, and R. J. Schoelkopf, "Programmable interference between two microwave quantum memories," Phys. Rev. X **8**, 021073 (2018).

[104] J. Q. You, X. Hu, S. Ashhab, and F. Nori, "Low-decoherence flux qubit," Phys. Rev. B **75**, 140515(R) (2007).

[105] F. Yan, S. Gustavsson, A. Kamal, J. Birenbaum, A. P. Sears, D. Hover, T. J. Gudmundsen, D. Rosenberg, G. Samach, S. Weber, J. L. Yoder, T. P. Orlando, J. Clarke, A. J. Kerman, and W. D. Oliver, "The flux qubit revisited to enhance coherence and reproducibility," Nat. Commun. **7** (2016).

[106] M. Stern, G. Catelani, Y. Kubo, C. Grezes, A. Bienfait, D. Vion, D. Esteve, and P. Bertet, "Flux qubits with long coherence times for hybrid quantum circuits," Phys. Rev. Lett. **113**, 123601 (2014).

[107] J.-L. Orgiazzi, C. Deng, D. Layden, R. Marchildon, F. Kitapli, F. Shen, M. Bal, F. R. Ong, and A. Lupascu, "Flux qubits in a planar circuit quantum electrodynamics architecture: Quantum control and decoherence," Phys. Rev. B **93**, 104518 (2016).

SUPPLEMENTAL MATERIAL FOR "FAULT-TOLERANT MULTI-QUBIT GEOMETRIC ENTANGLING GATES USING PHOTONIC CAT QUBITS"

In this Supplemental Material, we first discus how to generate Schrödinger's cat states (i.e., superpositions of coherent states) in the pumped-cat oscillators (PCOs). These cat states are used in the main text as the input states for the Mølmer-Sørensen (MS) gate. Then, we show a simple example to realize single-qubit gates using the PCO. Moreover, we show a possible implementation for the PCO using superconducting quantum interference devices.

S1. PREPARING SCHRÖDINGER CAT STATES

To generate the quantum cat states in the pumped-cat oscillators (PCOs), we first decouple the PCOs from the common cavity a_0 by tuning $J = 0$ or $\Delta = \infty$. Then, we change the Hamiltonian for each PCO to be time-dependent (we assume $\Omega_p(t) = \Omega_p^*(t) \geq 0$ for simplicity)

$$H_n^{\mathrm{Kerr}}(t) = \Omega_p(t)\left(a_n^{\dagger 2} + a_n^2\right) - Ka_n^{\dagger 2}a_n^2 + \Delta_q(t)a_n^\dagger a_n, \qquad t \in [-t_0, 0] \tag{S1}$$

where $\Delta_q(t) = \omega_c - \omega_p/2$ is a time-dependent detuning and t_0 denotes the total evolution time required for the generation of cat states. To study the dynamics of the time-dependent Hamiltonian $H_n^{\mathrm{Kerr}}(t)$, we introduce the displacement operators $D_n(\pm\alpha_t) = \exp\left(\pm\alpha_t a_n^\dagger \mp \alpha_t a_n\right)$ to transform $H_n^{\mathrm{Kerr}}(t)$ as

$$H_n'(t) = D_n(\pm\alpha_t)H_n^{\mathrm{Kerr}}(t)D_n(\mp\alpha_t) - iD_n(\pm\alpha_t)\dot{D}_n(\mp\alpha_t)$$

$$= \left[\Delta_q(t) - 4K\alpha_t^2\right]a_n^\dagger a_n - Ka_n^{\dagger 2}a_n^2 \mp 2K\alpha_t\left(a_n^{\dagger 2}a_n + a_n^\dagger a_n^2\right) \mp \left[\alpha_t\Delta_q(t) + i\dot{\alpha}_t\right]a_n^\dagger \mp \left[\alpha_t\Delta_q(t) - i\dot{\alpha}_t\right]a_n, \tag{S2}$$

where $\alpha_t = \sqrt{\Omega_p(t)/K} \geq 0$ is the time-dependent amplitude of a coherent state $|\alpha_t\rangle$.

Obviously, when

$$\left[\Delta_q(t) - 4K\alpha_t^2\right] \gg 2K\alpha_t, \quad \text{and} \quad \sqrt{\left[\alpha_t\Delta_q(t)\right]^2 + \dot{\alpha}_t^2}, \tag{S3}$$

the Hamiltonian $H_n'(t)$ cannot change the photon number of the system in the displacement frame. In this case, when α_t satisfies the boundaries

$$\alpha_t|_{t=-t_0} = 0, \quad \text{and} \quad \alpha_t|_{t=0} = \alpha. \tag{S4}$$

Assuming that the system in the displaced frame is in the displaced vacuum state $|0\rangle_n$ at the time $-t_0$, the evolution in the lab frame can be described by

$$|\psi(t)\rangle_n = D_n(\pm\alpha_t)|0\rangle_n, \tag{S5}$$

or can be equivalently described by

$$|\psi(t)\rangle_n = \mathcal{N}_\pm(\alpha_t)\left[D_n(\alpha_t) \pm D_n(-\alpha_t)\right]|0\rangle_n, \tag{S6}$$

where $\mathcal{N}_\pm(\alpha_t) = 1/\sqrt{2\left[1 \pm \exp(-2\alpha_t^2)\right]}$.

For simplicity, we assume

$$\alpha_t = \begin{cases} \alpha(t + t_0)/t_0, \\ \alpha, \end{cases} \quad \text{and} \quad \Delta_q(t) = \begin{cases} -K\sin\left[\pi(t + t_0)/t_0\right], & (-t_0 < t \leq 0) \\ 0, & (t \geq 0) \end{cases} \tag{S7}$$

to satisfy the condition in Eq. (S3). Then, at $t = 0$, the desired cat states $|\mathcal{C}_\pm\rangle_n = |\psi(0)\rangle_n$ can be generated. The driving amplitude $\Omega_p(t)$ and the detuning $\Delta_q(t)$ using the parameters in Eq. (S7) are shown in Fig. S1(a). In the absence of decoherence, the fidelities $F_\pm = {}_n\langle\mathcal{C}_\pm|\rho(0)|\mathcal{C}_\pm\rangle_n$ of the prepared cat states are shown in Fig. S1(b) and Fig S1(c). As a result, an evolution time $t_0 \gtrsim 1.7/K \approx 3$ ns (when $K/2\pi = 10$ MHz) is enough to generate the cat states $|\mathcal{C}_\pm\rangle_n$ with fidelities $\gtrsim 99\%$. In the presence of decoherence, for the nth PCO, the dynamics is described by the Lindblad master equation

$$\dot{\rho}_n = -i[H_n^{\mathrm{Kerr}}(t), \rho_n] + \kappa\mathcal{D}[a_n]\rho_n + \gamma\mathcal{D}[a_n^\dagger a_n]\rho_n, \tag{S8}$$

where $\mathcal{D}[o]\rho_n = o\rho_n o^\dagger - \left(o^\dagger o\rho_n + \rho_n o^\dagger o\right)/2$ is the Lindblad superoperator, κ is the single-photon loss rate, and γ is the pure dephasing rate. In Fig. S1(b) and Fig. S1(c), we can see that the fidelities of the cat states can be higher than 95% when the decay rates are $\kappa = \gamma = 0.01K$.
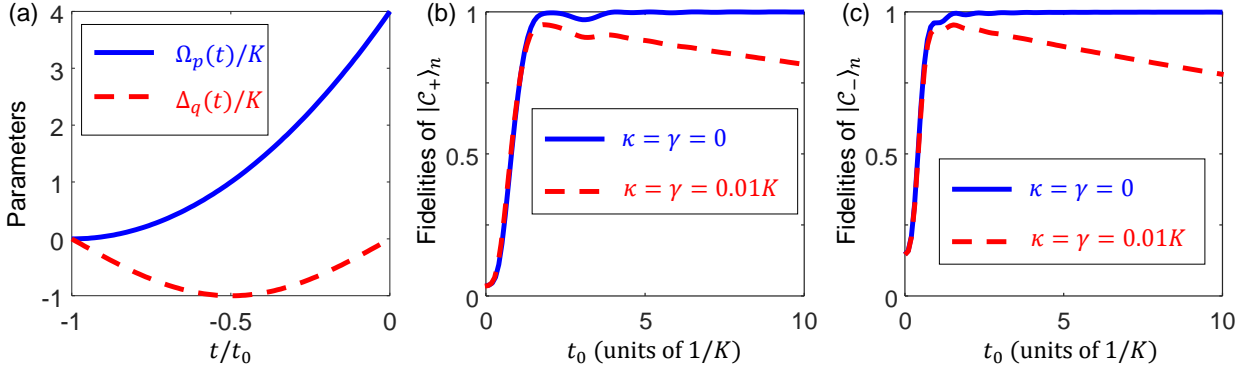
FIG. S1. (a) Parameters used for the generation of the cat states $|\mathcal{C}_\pm\rangle_n$. Fidelities of (b) the even cat state $|\mathcal{C}_+\rangle_n$ and (c) the odd cat state $|\mathcal{C}_-\rangle_n$ versus the total evolution time t_0. The initial states for (b) is $|\psi(-t_0)\rangle_n = |0\rangle_n$ and (c) is $|\psi(-t_0)\rangle_n = |1\rangle_n$. Other parameters are given in Eq. (S7).

S2. ARBITRARY SINGLE-QUBIT ROTATIONS OF CAT QUBITS

Accompanied by a variety of single-qubit rotations, the Mølmer-Sørensen gate can be adapted to many quantum algorithms, such as Grover's quantum search algorithm [3, 52, 53]. To realize such single-qubit rotations, one needs to add a single-photon drive to each PCO [70]. The Hamiltonian for each PCO becomes

$$\tilde{H}_n^{\text{Kerr}} = \Omega_p \left(a_n^{\dagger 2} + a_n^2\right) - K a_n^{\dagger 2} a_n^2 + \Delta_q a_n^\dagger a_n + (\xi_p a_n + \xi_p^* a_n^\dagger), \tag{S9}$$

where ξ_p is the complex driving amplitude. Note that the parameters discussed in this section are independent of those in the main text and Sec. S1. When $\Delta_q, |\xi_p| \ll E_{\text{gap}} = 4\alpha^2 K$, the evolution is restricted in the cat-state subspace $\mathcal{C}$. The effective Hamiltonian in the cat-subspace reads ($\alpha = \alpha^* = \sqrt{\Omega_p/K}$):

$$\begin{aligned}
\tilde{H}_{n,\text{eff}}^{\text{Kerr}} =& \frac{1}{2}\Delta_q \alpha^2 \left(\coth\alpha^2 - \tanh\alpha^2\right) \sigma_n^z \\
&+ \left(\xi\alpha\sqrt{\tanh\alpha^2} + \xi^*\alpha\sqrt{\coth\alpha^2}\right) \sigma_n^- + \left(\xi^*\alpha\sqrt{\tanh\alpha^2} + \xi\alpha\sqrt{\coth\alpha^2}\right) \sigma_n^+ \\
=& \frac{\tilde{\Delta}_q}{2}\sigma_n^z + \Omega_1 \exp\left(-i\varphi\right)\sigma_n^- + \Omega_1 \exp\left(i\varphi\right)\sigma_n^+, \tag{S10}
\end{aligned}$$

where $\sigma_n^z = |\mathcal{C}_-\rangle_n\langle\mathcal{C}_-| - |\mathcal{C}_+\rangle_n\langle\mathcal{C}_+|$.

Obviously, the effective Hamiltonian $\tilde{H}_{n,\text{eff}}^{\text{Kerr}}$ contains all the Pauli matrixes for a two-level system. Thus, it can realize arbitrary single-qubit rotations. The evolution operator in matrix form becomes

$$U_1 = \exp\left(-i\tilde{H}_{n,\text{eff}}t\right) = \begin{pmatrix} \cos(\Xi t) - i\sin(\Xi t)\cos\theta & -i\exp\left(-i\varphi\right)\sin(\Xi t)\sin\theta \\ -i\exp\left(i\varphi\right)\sin(\Xi t)\sin\theta & \cos(\Xi t) + i\sin(\Xi t)\cos\theta \end{pmatrix}, \tag{S11}$$

which denotes an arbitrary rotation on the Bloch sphere [see Fig. S2(a)]. Here, $\Xi = \sqrt{\tilde{\Delta}_q^2/4 + \Omega_1^2}$ and $\theta = \arctan(2\Omega_1/\tilde{\Delta}_q)$. For instance, when $\Xi t = \pi/2$, $\theta = \pi/4$, and $\varphi = 0$, U_1 denotes the Hadamard gate up to a global phase $\pi/2$ [see the blue-dashed curve in Fig. S2(b)]. When $\Xi t = \pi/2$, $\theta = \pi/2$, and $\varphi = 0$, U_1 becomes the NOT gate up to a global phase $\pi/2$ [see the red-solid curve in Fig. S2(b)]. We can see in Fig. S2(b) that the gate time of the Hadamard gate is much longer than that of the NOT gate. This is understood because the effective detuning $\tilde{\Delta}_q$ exponentially decreases when α increases. Thus, it takes a long time to obtain a phase rotation about the z axis.

As an alternative to obtaining a large effective detuning $\tilde{\Delta}_q$, one can employ an interaction Hamiltonian

$$H_{\text{add}}(t) = \xi_J \cos\left[\varphi_a(a_n e^{-i\omega_c t} + a_n^\dagger e^{i\omega_c t})\right] = \frac{\xi_J}{2}\left[D_n(\beta_t) + D_n(-\beta_t)\right], \qquad \beta_t = i\varphi_a \exp\left(i\omega_c t\right), \tag{S12}$$

which can be realized by strongly coupling a high impedance cavity mode to a Josephson junction [71–73]. Here, ξ_J is the effective Josephson energy and $\varphi_a = \sqrt{Z_a/2R_Q}$, with Z_a and R_Q being the impedance of the cavity mode seen
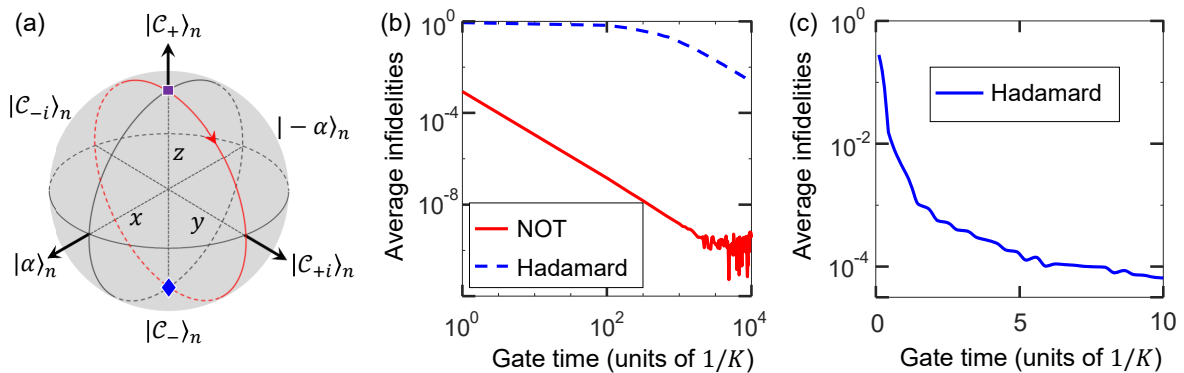
FIG. S2. (a) Bloch sphere of the cat qubit in the limit of large α (i.e., $\alpha = 2$). The red circle with a red arrow denotes the evolution path for the NOT gate. For instance, when the input state is $|\mathcal{C}_+\rangle_n$ (purple square), the NOT gate transforms this input state into $|\mathcal{C}_-\rangle_n$ (blue diamond). The states on all y axis are $|\mathcal{C}_{\pm i}\rangle_n \simeq (|\alpha\rangle_n \pm i|-\alpha\rangle_n)/\sqrt{2}$. (b) Average infidelities of the Hadamard and NOT gates versus the gate time calculated via the Hamiltonian in Eq. (S9). (c) Average infidelities of the Hadamard gate when the additional Hamiltonian in Eq. (S12) is added, i.e., when the total Hamiltonian is $H_{\mathrm{tot}}(t) = \tilde{H}_n^{\mathrm{Kerr}} + H_{\mathrm{add}}(t)$. We assume that the frequency of each PCO is $\omega_c = 800K$ and the coherent-state amplitude is $\alpha = 2$. Other parameters are given below Eq. (S11).

by the junction and the superconducting resistance quantum, respectively. When $\omega_c, E_{\mathrm{gap}} \gg \xi_J$ and $\varphi_a \simeq 2\alpha$, the effective Hamiltonian under the rotating wave approximation in the cat-state becomes reads [73]

$$\tilde{H}_{\mathrm{add}} = \frac{\tilde{\Delta}_q}{2}\sigma_n^z, \tag{S13}$$

where $\tilde{\Delta}_q \simeq \xi_J/\alpha\sqrt{2\pi}$. Substituting Eq. (S13) into Eq. (S10) and assuming $\Delta_q = 0$, the evolution operator still takes the form of Eq. (S11). Figure S2(c) shows the average infidelities of the Hadamard gate when the additional Hamiltonian $H_{\mathrm{add}}(t)$ is added. Comparing to the result in Fig. S2(b), the additional Hamiltonian $H_{\mathrm{add}}(t)$ obviously increases the effective detuning, so that the gate time is shortened. For instance, a gate time $\sim 5/K \approx 8$ ns (for $K/2\pi \sim 10$ MHz) is enough to achieve a Hadamard gate with a fidelity $\gtrsim 99.99\%$.

S3. A POSSIBLE IMPLEMENTATION USING SUPERCONDUCTING QUANTUM INTERFERENCE DEVICES

As shown in Fig. S3, an array-type resonator composed of N_0 superconducting quantum interference devices (SQUIDs) [95, 96] can be used to realize the Hamiltonian for the PCOs. The Hamiltonian for the setup in Fig. S3 reads

$$H_0 = 4E_C\hat{n}^2 - N_0 E_J[\Phi(t)]\cos\frac{\hat{\phi}}{N_0}, \tag{S14}$$

where $\hat{n}$ and $\hat{\phi}$ are the number of Cooper pairs and the overall phase across the junction array, respectively. E_C and E_J are the resonator's charging energy and the Josephson energy of a single SQUID, respectively. $\Phi(t)$ is the external magnetic flux for periodically modulating (with a frequency ω_p) the Josephson energy, which is modified to be

$$E_J[\Phi(t)] = E_J + \delta E_J \cos(\omega_p t). \tag{S15}$$

After the Taylor expansion of $\cos\left(\hat{\phi}/N_0\right)$ to fourth order, we obtain

$$H_0 \approx 4E_C\hat{n}^2 - N_0 E_J(1 - \hat{X} + \hat{X}^2/6) - N_0\delta E_J(1 - \hat{X})\cos(\omega_p t), \tag{S16}$$

where $\hat{X} = (\hat{\phi}/N_0)^2/2$. Then, we can define two operators

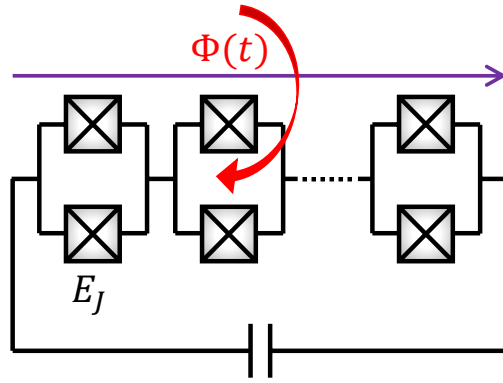$$\hat{n} = -in_0(a - a^\dagger), \qquad \hat{\phi} = \phi_0(a + a^\dagger), \tag{S17}$$

FIG. S3. Superconducting quantum circuit for implementing the PCOs. The circuit consists of a SQUID array (black), a shunting capacitor (black), and a flux bias line (purple). Here, $\Phi(t)$ is the externally applied magnetic flux and E_J is the Josephson energy of a single SQUID.

where $n_0 = \sqrt[4]{E_J/(32N_0E_C)}$ and $\phi_0 = 2\sqrt{2}/n_0$ are the zero-point fluctuations. The quadratic time-independent part of the Hamiltonian H_0 can be diagonalized and the Hamiltonian H_0 becomes ($\hbar = 1$)

$$H_0 = \omega_c a^\dagger a - \frac{E_C}{12N_0^2}\left(a + a^\dagger\right)^4 + \frac{\delta E_J \omega_c}{4E_J}\left(a + a^\dagger\right)^2 \cos(\omega_p t), \tag{S18}$$

where $\omega_c = \sqrt{8E_C E_J/N_0}$. Here, we have dropped the constant terms for simplicity.

Moving into a rotating frame at the frequency of $\omega_p/2$, we obtain

$$\begin{aligned}H_0 = &\Delta_0 a^\dagger a - \frac{E_C}{12N_0^2}\left[a\exp(-i\omega_p t/2) + a^\dagger \exp(i\omega_p t/2)\right]^4 \\ &+ \frac{\delta E_J \omega_c}{4E_J}\left[a\exp(-i\omega_p t/2) + a^\dagger \exp(i\omega_p t/2)\right]^2 \cos(\omega_p t).\end{aligned} \tag{S19}$$

When the conditions

$$\omega_p \gg \frac{E_C}{12N_0^2}, \qquad \text{and} \qquad \omega_p \gg \frac{\delta E_J \omega_c}{4E_J}, \tag{S20}$$

are satisfied, the counter-rotating terms in Eq. (S19) can be neglected. The effective Hamiltonian of the system becomes

$$H_{\text{Kerr}} = \Delta_q a^\dagger a - K a^{\dagger 2} a^2 + \Omega_p (a^{\dagger 2} + a^2), \tag{S21}$$

where $\Delta_q = \Delta_0 - 2K$, $K = 2E_C/N_0^2$, and $\Omega_p = \delta E_J \omega_c/8E_J$. Hence, we obtain the Hamiltonian [i.e., Eq. (1) of the main text] for the PCOs.